Journal of Applied Electrochemistry **30**: 467–474, 2000.

Electrochemical behaviour of olefins: oxidation at ruthenium–titanium dioxide and iridium–titanium dioxide coated electrodes

C.L.P.S. ZANTA[1], A.R. de ANDRADE[1]* and J.F.C. BOODTS[2]
[1]*Chemistry Department, FFCLRP-USP, Universidade de São Paulo, Av. Bandeirantes 3900, 14040-901, Ribeirão Preto, SP, Brazil*
[2]*Chemistry Department Universidade Federal de Uberlândia, Av. João Naves de Ávila 2160, 38400-902, Uberlândia, MG, Brazil*
*(*author for correspondence)*

Received 17 February 1999; accepted in revised form 19 October 1999

Key words: catalytic activity, iridium dioxide, olefins, oxide electrodes, ruthenium dioxide

Abstract

The electrocatalytic behaviour of a series of olefins was studied on thermally prepared Ti/MO_2 and $Ti/M_{0.3}Ti_{0.7}O_2$ electrodes (M = Ru, Ir) in 1.0 M $HClO_4$ in mixed solvent (AN/H_2O, 40/60 v/v). The voltammetric investigation was limited to the potential region preceding the OER on these electrodes materials ($E < 1.2$ V vs SSCE). Aliphatic olefins (isophorone and cyclohexene) are inactive while the aromatic olefins show a single (safrole) or two (isosafrole) oxidation peaks. The overall catalytic activity of these electrode materials is about the same for both substrates. However, when morphological effects (differences in electrode surface area) are taken into account, normalizing the geometric current density (or faradaic charge) per surface site activity, a slightly better efficiency of the active surface sites is observed for Ru-based electrodes when compared to the equivalent Ir-based materials. Partial substitution of the noble metal catalysts by TiO_2 results in a synergetic effect depressing the efficiency of the active surface sites of the TiO_2-stabilized electrocatalysts. The decrease with potential cycling of the substrate oxidation current is attributed to dimeric/polymeric film formation blocking the electrode surface. Reflectance and FTIR spectroscopy as well as ohmic resistance data support film formation.

1. Introduction

Oxidation is one of the most widely used synthetic procedures to introduce structural changes in organic substrates. Although the classical organic synthetic routes make use of oxidants which are frequently expensive, dangerous and environmentally unfriendly (e.g., transition metal compounds), heterogeneous electrocatalytic routes have the advantage of employing oxidants immobilized in the electrode material thus resulting in a cleaner procedure which, additionally, reduces the subsequent elaboration steps needed to isolate the products.

DSA® electrodes, basically consisting of Ti-supported, TiO_2-stabilized, noble metal oxides having rutile structure [1] show some highly desirable features: (i) high surface area (roughness) which can be easily modified; (ii) excellent mechanical, electrical and electrocatalytic properties; (iii) the experimentally accessible potential interval can be easily changed; (iv) the catalyst is immobilized; (v) catalytic properties can be modulated introducing a modulating oxide (binary and ternary oxide mixtures); (vi) DSA® are good catalysts for chlorine and oxygen formation and therefore these reactions can be explored to introduce structural modifications in organic substrates; and (vii) DSA® are commercially available and are environmental friendly electrode materials. These features make DSA® interesting electrode materials for application in organic electrooxidation and have stimulated activity in this field [2–8]. The Ti/RuO_2 system has received considerable attention due to its excellent stability, electrocatalytic properties and also the oxide coating prevents Ti-passivation [9]. A further advantage is the large number of Ru-oxidation states existing at the electrode surface in the potential region between the hydrogen evolution reaction, HER, and the oxygen evolution reaction, OER [10, 11]. Among them the Ru(VI)/Ru(VII) (ruthenate/perruthenate) redox couple has been pointed as an excellent mediator due its good reversibility and stability [11, 12]. The better resistance to anodic corrosion has stimulated interest in Ti/IrO_2 when compared to the Ti/RuO_2 electrode [12].

Despite its favourable properties, DSA® has been only marginally explored in organic electrosynthesis [13]. In the 1970s, the first paper on organic oxidation using oxide electrodes was published by Galizzioli et al. [14]. More recently, these electrode materials have

become intensively explored in the organic electrosynthesis [2, 4–6] and wastewater treatment fields [15–17]. Due to their importance in fuel cell applications, most of the published work has been centred on the oxidation of alcohols and aldehydes while some work investigating the oxidation of slightly larger, more complex, organic substrates has appeared [5, 7, 18]. We therefore decided to investigate Ti/MO_2 and $Ti/M_{0.3}Ti_{0.7}O_2$ (M = Ru or Ir) electrodes with respect to their activity towards the oxidation of aromatic (safrole, SF, and isosafrole, ISF) and aliphatic (cyclohexene, CH, and isophorone, IS) olefins. The substrates were chosen to study the influence of the organic structure on the oxidation process.

It is very important to find economically viable synthetic routes that convert starting materials to value-added products. For instance, the main oxidation product of ISF is piperonal, PI, a widely used product in the perfume industry. Large-scale production of PI involves Cr(VI) as an oxidant [19]. Although economically feasible, the use of Cr(VI) is a drawback. Alternative production processes have been investigated, for example, homogeneous electrocatalysis using a Ru(IV) pyridine complex [20] and more recently direct oxidation with PbO_2 or indirect oxidation with MnO_2 as proposed by Grimshaw and Hua [21]. PI yields of 48.9% [20] and 54% [21] in indirect oxidation and 35% [21] in direct oxidation were obtained.

2. Experimental details

2.1. *Preparation of electrodes materials*

Electrodes materials were prepared by thermal decomposition ($T_{calcination}$: 400 °C; 1 h; oxygen flux: 5 $dm^3\,min^{-1}$) of the appropriate precursor mixtures prepared in HCl 1:1 (v/v). Chlorides were used as precursor salts ($RuCl_3.nH_2O$ Aldrich, $TiCl_4$ 99% Vectron, $IrCl_3.nH_2O$ Aldrich), which were applied by brush to both sides of the pretreated Ti-support (10 mm × 10 mm × 0.13 mm) to achieve a 2 μm thick coating, corresponding to 1.0–2.3 mg cm^{-2} oxide loading (depending on composition). An average of four or five applications was required to obtain the desired oxide loading. Details of the preparation and final mounting of the electrode are described elsewhere [22].

2.2. *Solvent*

Acetonitrile, AN, was used as co-solvent in an AN/H_2O, 40/60 (v/v) ratio to obtain the desired solubility of the substrates (~0.1 M). Substrates investigated (all Aldrich) were purified by distillation.

2.3. *Cell and equipment*

All experiments were conducted with a Princeton Applied Research (PARC, model 273A) potentiostat/galvanostat controlled by M270 software. A home-made three compartments cell consisting of a main body (~200 mL) and two smaller compartment, isolated from the main body by coarse glass frits, containing two platinized platinum wires employed as auxiliary electrodes, was used throughout. The reference electrode was a sodium saturated calomel electrode, SSCE. Infrared spectra were recorded on a Nicolet (model 5ZDX) FTIR spectrometer. Reflectance electronic spectra were obtained using a Guided Wave (model 260) optic fibre spectrometer equipped with tungsten–halogen lamps and silicon (u.v.–vis.) and germanium (near i.r.) detectors. Electrochemical impedance spectra were obtained covering the 5 mHz to 100 kHz frequency interval, employing a PARC (model 5210) lock-in amplifier, coupled to the 273A potentiostat/galvanostat.

3. Results and discussion

3.1. *Voltammetric characterisation of the electrode materials*

The standard method for *in situ* characterization of this kind of electrode material is recording CV, at 20 mV s^{-1}, from 1.0 M $HClO_4$ covering the potential region before the onset of the HER (0.4 V vs RHE) and the beginning of OER (1.4 V vs RHE) [23]. In this potential region the observed voltammetric current is the sum of the solid state surface redox transitions (the main contribution) and the double layer charging. In the case of ruthenium and iridium, the later process represents only a minor contribution to the total current. Therefore, integration of the i/E curve results in the voltammetric charge, q^*, which can be taken as a relative measure of the number of electrochemically active site [24, 25]. Table 1 shows the q^* values as a function of the oxide composition investigated. The voltammetric behaviour of these materials in aqueous acid conditions is well-known [10, 26]. However, almost no information about the voltammetric behaviour in mixed aqueous/organic solvent is available making a characterisation of the system under these conditions necessary. Representative CVs, recorded between 0 and 1.1 V vs SSCE using standard conditions, are shown in Figure 1. The voltammetric behaviour of Ti/MO_2 and $Ti/M_{0.3}Ti_{0.7}O_2$ (M = Ru, Ir) electrodes in AN/H_2O, 40/60 v/v, mixed solvent is similar to the behaviour observed in aqueous medium (1.0 M $HClO_4$), showing that the organic co-solvent, at least at the concentration used, exerts no influence on the electrochemical behaviour of the electrodes.

Table 1. Voltammetric charge as a function of the composition of the electrode obtained by integration of the voltammetric curve, recorded in the absence of substrate, over the 0–1.1 V vs SSCE potential interval

Electrode	RuO_2	IrO_2	$Ru_{0.3}Ti_{0.7}O_2$	$Ir_{0.3}Ti_{0.7}O_2$
Charge, q^* /mC cm^{-2}	6.0	10.1	13.3	91.5

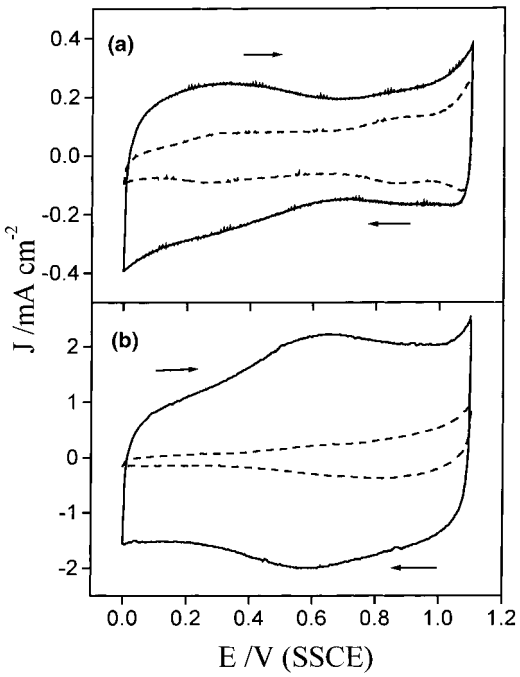

Fig. 1. Representative cyclic voltammograms in 1.0 M $HClO_4$ and AN/H_2O 40/60 (v/v) of: (a) (——) $Ti/Ru_{0.3}Ti_{0.7}O_2$, (- - - - -) Ti/RuO_2 and (b) (——) $Ti/Ir_{0.3}Ti_{0.7}O_2$, (- - - - -) Ti/IrO_2. $v = 20$ mV s^{-1}, $A = 2.0$ cm^2.

In agreement with the known behaviour [2, 26], the Ti/RuO_2 electrode shows a pair of broad, not well-defined, bands in the 0.2–0.4 V vs SSCE potential region, associated with Ru(III)/Ru(IV) solid state redox transition. A second less pronounced anodic band, centred around 0.9 V vs SSCE and associated with the Ru(IV)/Ru(VI) redox transition, is also observed. The partial substitution of RuO_2 by TiO_2, frequently used to stabilize the Ti/RuO_2 electrode and to reduce cost (lower noble metal loading with only a slight loss in electrocatalytic activity), results in the following modifications of the voltammetric behaviour: (i) the voltammetric charge, q^*, increases from 6.0 to 13.3 mC cm^{-2} when 70% of RuO_2 is substituted by TiO_2; (ii) the Ru(IV)/Ru(VI) solid state redox transition becomes less pronounced.

The i/E curve (Figure 1) shows, for Ir-based electrode materials, only the Ir(III)/Ir(IV) solid state transition, localized at 0.4–0.8 V vs SSCE. Nevertheless, Wen and Hu [26] observed evidences of Ir(IV)/Ir(VI) transition states before the onset of OER. The partial substitution of IrO_2 by TiO_2 leads to a drastic increase in q^* from 10.1 mC cm^{-2}, for the pure catalyst, to 91.5 mC cm^{-2} for the binary system. A systematic SEM investigation of the $Ti/Ir_xTi_{(1-x)}O_2$ system by da Silva et al. [27] showed that a very rough structure is obtained for intermediate compositions ($0.4 \leqslant x \geqslant 0.8$). IrO_2 segregation from binary or higher mixed oxide systems is a well-known phenomenon [27, 28]. Thus the drastic increase in voltammetric charge (number of electrochemically active sites) can be attributed to an increase in roughness of the binary system combined with IrO_2-segregation.

3.2. *Oxidation of organic substrates*

Figure 2 shows the structural formula of the organic molecules investigated. Aromatic and aliphatic olefins in acid mixed solvent behave rather differently on DSA®. No voltammetric current was observed with the aliphatic olefins (CH and IS) showing that the electrode materials under investigation, and at the experimental conditions explored, do not possess electrocatalytic activity for this group of substrates. In the case of the aromatic olefins (SF and ISF), however, high oxidation currents were obtained, as shown in Figures 3 and 4. The aromatic substrates behave differently in the sense that, while for all conditions explored SF gives a single well defined irreversible oxidation peak, with $E_p \simeq 1.05$ V (Figure 3), ISF furnished two well defined irreversible oxidation waves with peak potentials

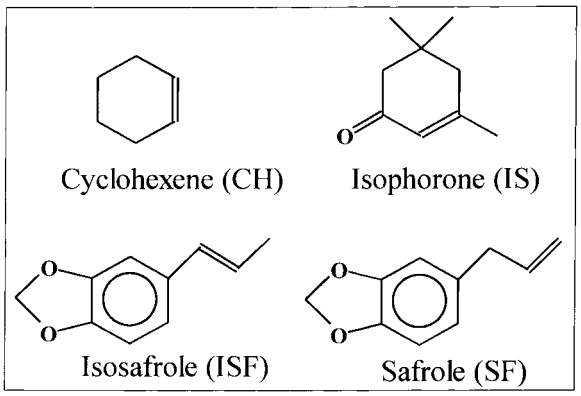

Fig. 2. Substrates investigated.

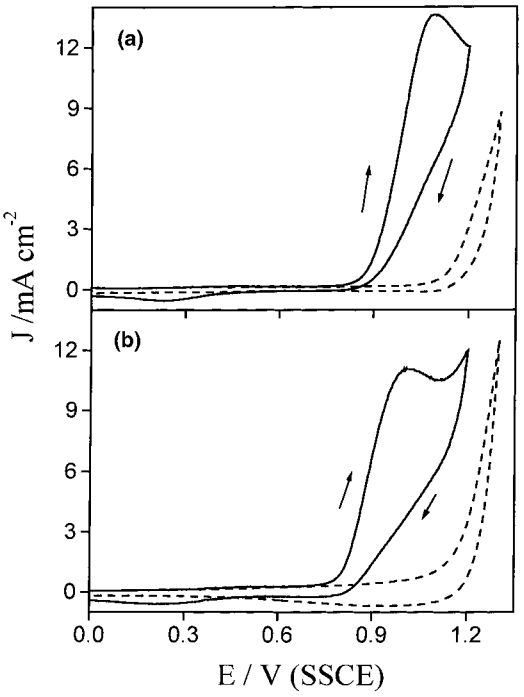

Fig. 3. Representatives cyclic voltammograms (- - - - -) in the absence; (——) in the presence of 33 mM SF in 1.0 M $HClO_4$ and AN/H_2O 40/60 (v/v). (a) Ti/RuO_2; (b) Ti/IrO_2. $v = 20$ mV s^{-1}, $A = 2.0$ cm^2.

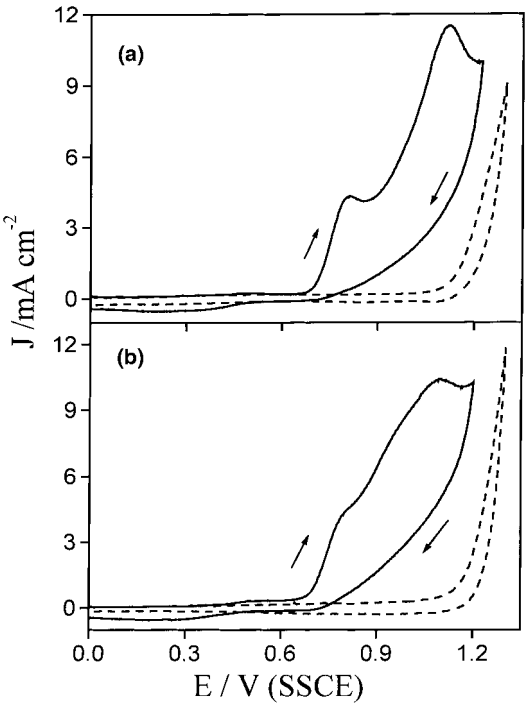

Fig. 4. Representatives cyclic voltammograms (- - - - -) in the absence; (—) in the presence of 36 mM ISF in 1.0 M $HClO_4$ and AN/H_2O 40/60 (v/v). (a) Ti/RuO_2; (b) Ti/IrO_2. $v = 20$ mV s^{-1}, $A = 2.0$ cm^2.

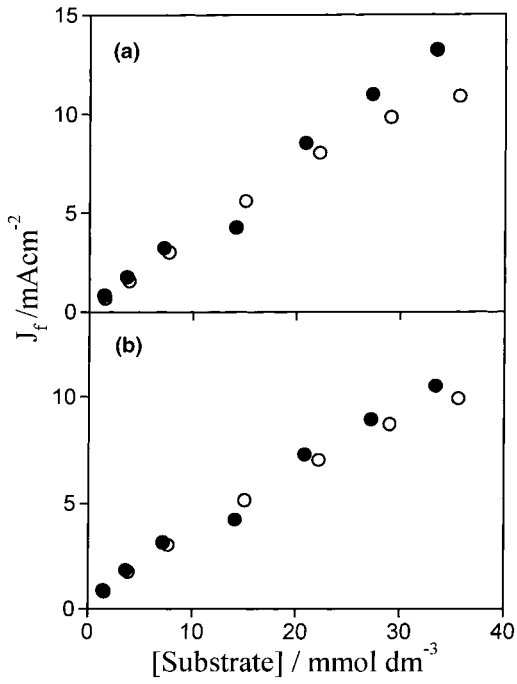

Fig. 5. Faradaic current density as a function of substrate concentration. 1.0 M $HClO_4$ in AN/H_2O 40/60 (v/v). (a) Ti/RuO_2; (b) Ti/IrO_2; (●) SF and (○) ISF (for ISF $J_f = J_{f,peak\,1} + J_{f,peak\,2}$).

respectively at 0.8 and 1.10 V (Figure 4). Partial substitution of the catalysts (RuO_2 or IrO_2) by TiO_2 does not significantly affect this behaviour.

The fact that the aromatic olefins are more easily oxidized can be understood considering the negative charge density, δ^-, induced by the aromatic ring and the presence of the two oxygen atoms in the structure. The difference in electrochemical behaviour between SF and ISF can be explained in terms of the conjugation present in the ISF structure. While the cation radical of the conjugated olefin (ISF), formed after the first oxidation process, is stabilised through ring conjugation, thus requiring a more anodic potential (more energy) for further oxidation, no such charge stabilisation occurs with the nonconjugated SF. Thus both oxidation processes occur at about the same potential, resulting in a single oxidation peak.

In the case of the Ti/RuO_2 electrode the substrate oxidation processes coincide with the potential region where the Ru(IV)/Ru(VI) solid state redox process occurs [2, 26]. Thus the catalytic species may be associated with the ruthenate (RuO_4^{-2}) form. With the Ti/IrO_2 electrode, organic substrates are oxidised at slightly more anodic potentials than the Ir(III)/Ir(IV) transition, suggesting the oxidation process involves higher oxidation states than Ir(IV). A similar conclusion was reached by O'Sullivan and White [2].

3.3. *Efficiency for substrate oxidation*

Figure 5 shows the faradaic current densities, J_f, as a function of substrate concentration for the pure oxide electrodes. The faradaic current density, J_f, due to the organic substrate oxidation, was obtained subtracting the total current density, J_{total} (measured at the peak potential or plateau) from the current density due to the solid state redox transition, J_{se}, so: $J_f = J_{total} - J_{se}$. The J_{se} values were obtained from a CV recorded with the pure supporting electrolyte and measured at the same potential of J_{total}. In the case of ISF J_f represents the total current (sum of peak 1 and peak 2). From the data of Figure 5, an apparent reaction order with respect to the SF and ISF concentration of ~1 was derived for both catalyst materials. Iridium oxide electrodes showed a slightly smaller value (0.8) reflecting the somewhat stronger adsorption of the organic material compared with RuO_2.

A comparison of the graphs of Figure 5 shows a linear relationship and approximately the same current density at low substrate concentration (<20 mM) for both electrode materials. Since both substrates have very similar structures it is reasonable to assume similar diffusion coefficients and degrees of accessibility to the electrode surface, suggesting the total number of electrons involved in the oxidation process of both substrates to be the same. At higher substrate concentrations, a slightly different behaviour is observed. For both electrode materials J_f values for SF continue to increase in an almost linear manner with concentration, while the current levels off in the case of ISF. In principle, the behaviour at the higher ISF concentrations may be attributed to current limitation due to mass transport. This, however, does not explain why SF behaves differently from ISF at the higher substrate concentration. Continuous potential cycling

experiments (following Section) show that the electrode surface is blocked by film formation due to radical dimerization/polymerization. Dimerization and polymerization are higher order processes explaining why blocking of the electrode surface only becomes an important feature at the higher substrate concentrations, while the difference in cation radical stability explains the more pronounced effect observed with ISF. In fact the higher stability of the ISF radical permits a higher radical concentration at the electrode interface and explains why film formation is more pronounced for this substrate.

An approach to compare the efficiency of the surface active sites of different solid state electrode materials is the use of the faradaic voltammetric charge, q_f, instead of the faradaic current density. The use of q_f includes a much broader experimental universe compared with just one single experimental point used for J_f analyses. Besides the intrinsic, more important, statistical significance of q_f, events can be observed which frequently escape from a single-point analysis. q_f values were obtained by integrating the i/E curves over the potential interval between $E_i = 0.6$ V (at the foot of the oxidation processes) and the final potential, E_f, taken 50 mV more anodic then the peak potential (or the levelling-off of the current in cases where a plateau is observed). This integration results in the total voltammetric charge, q_{total}, from which the contribution of the redox transition, q_{se}, (obtained integrating the i/E curve recorded with a pure supporting electrolyte over the same potential interval) is subtracted, thus furnishing the faradaic charge due to substrate oxidation ($q_f = q_{total} - q_{se}$). Figure 6 shows q_f as a function of substrate concentration for all electrode materials investigated. Besides, the difference observed in the q^*-value (Table 1), the q_f against organic substrate concentration plot (Figure 6) is independent of the electrode material, showing the process is controlled by diffusion.

Q_f reflects both the apparent (morphological effect) and the real (efficiency of the surface active sites) efficiency and is a useful criteria to judge the overall efficiency of different substrates. However, and when the process is not totally surface controlled it cannot be used. In fact, the voltammetric charge (q^*) for the same geometric area (2 cm^2) shows a rather different values for the number of electrochemically active sites as the electrode composition is changed (Table 1). To obtain an useful criteria to judge the real efficiency of different electrode materials, one must eliminate the contributions due changes on the surface area. For oxide-based electrode materials an adequate approach is obtained dividing the faradaic voltammetric charge (q_f) by q^* (voltammetric charge obtained in the absence of organic substrate and a representative parameter of the number of active surface sites). The resulting normalised faradaic voltammetric charge, $q_{f,N}$, ($q_{f,N} = q_f/q^*$) is a parameter whose numerical value describes the faradaic charge per active surface site. Figure 7 shows $q_{f,N}$ as a function of substrate concentration.

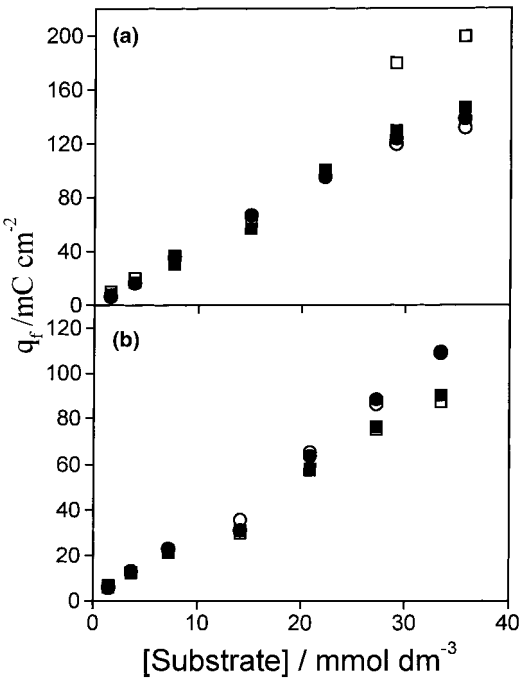

Fig. 6. Faradaic voltammetric charge as a function of substrate concentration. q_f obtained by integration of the i/E curve recorded in 1.0 M $HClO_4$ in AN/H_2O 40/60 (v/v), $v = 20$ mV s^{-1}. (a) ISF and (b) SF; (●) Ti/RuO_2; (○) Ti/$Ru_{0.3}Ti_{0.7}O_2$; (■) Ti/IrO_2; (□) Ti/$Ir_{0.3}Ti_{0.7}O_2$.

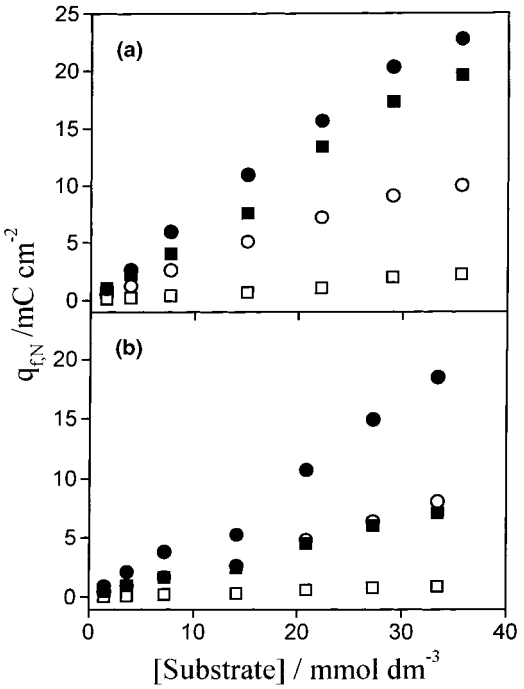

Fig. 7. Normalized faradaic voltammetric charge ($q_{f,N}$) as a function of substrate concentration. (a) ISF; (b) SF; (●) Ti/RuO_2; (○) Ti/$Ru_{0.3}Ti_{0.7}O_2$; (■) Ti/IrO_2; (□)Ti/$Ir_{0.3}Ti_{0.7}O_2$. (Voltammetric charge integrated from CV registered in the same conditions described in Figure 6).

The normalized faradaic voltammetric charge, $q_{f,N}$, shows some interesting features. (i) The normalized faradaic voltammetric charge is much higher for the

pure oxides than for the binary TiO_2 containing mixtures. This result suggests TiO_2 is capable of depressing the catalytic activity of the pure catalysts. (ii) The efficiency of the active surface sites of the Ti/RuO_2-electrodes is slightly better than Ti/IrO_2. It is worthwhile to stress that other fundamental properties (e.g., service life) should be considered before deciding which is the best electrode material for a given application.

3.4. *Investigation of the influence of continuous potential cycling*

Deactivation of DSA® in the presence of organic substrates and solvents has been reported in the literature [29]. Initially the influence of the organic solvent on the electrode behaviour was investigated by continuous cycling of the electrode potential between 0.1 and 1.2 V in 1.0 M $HClO_4$ and AN/H_2O, 40/60 v/v. During the first 40 cycles a gradual decrease of the current at the OER region ($E \approx 1.2$ V) was observed. Further increase of the number of potential cycles causes no change in the performance of the electrode. The small current decrease observed during the first 40 cycles can be attributed to an accommodation of the outer region of the oxide layer. Thus it seems a good practice to submit freshly prepared electrodes to a continuous potential cycling program until a reproducible i/E profile is obtained to assure that electrochemical active sites reaches an equilibrium state.

The continuous potential cycling investigation was also done in the presence of 33 mM SF (36 mM ISF). To minimise mass transport problems CVs were recorded using a strong N_2-flux. A representative result is showed in Figure 8.

For both substrates and electrode materials the results show that after 30 potential cycles oxidation process is almost completely blocked. Following possibilities were considered to explain the current decrease as function of the number of potential cycles: (i) electrode lixiviation; (ii) decrease of substrate concentration; (iii) blocking of the electrode surface. The first possibility can be excludes once after cleaning the blocked electrode, with an organic solvent (propanone), the original electrode activity is restored. In fact, identical q^*-values were obtained before blocking of the electrode surface and after its cleaning.

In view of the rather large electrodes used substrate consumption was also considered. Assuming $n = 2$, calculation of the charge consumed during 30 potential cycles resulted in substrate consumption values in the range of 5.0–7.2 mg. These values, compared with the original substrate mass (~330 mg) and considering that the solution was heavily stirred with a N_2-stream during the recording of the CV profiles permits to discard substrate concentration changes at the electrode/solution interface as a possible cause of the current decrease.

Blocking the electrode surface due the adsorption of organic substrate and/or dimeric/polymeric film formation is a well known feature of oxidation processes at solid electrodes. In the present investigation, blocking of the electrode activity by a film which covers its surface is the most probable cause of current decrease. The fact that electrode cleans choosing an appropriate organic solvent restoring its activity is good evidence in favour of surface blocking due to dimeric/polymeric film formation.

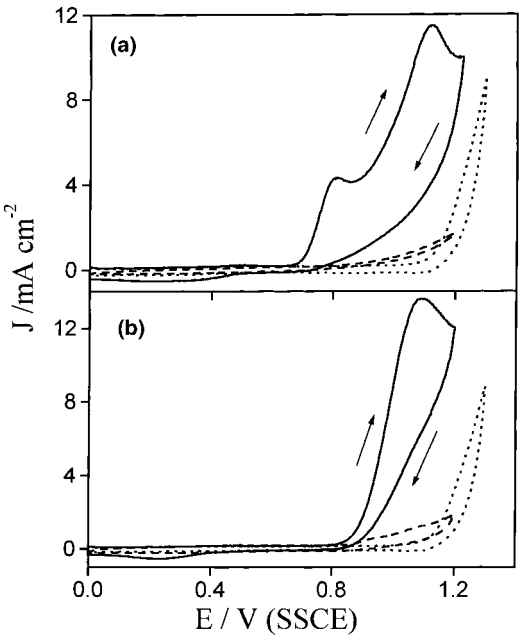

Fig. 8. Voltammetric curves as a function of continuous potential cycling in the presence of the organic substrate. (a) 36 mM ISF and (b) 33 mM SF. (——) first cycle; (- - - - - -) 30th cycle; (· · · · · ·) in support electrolyte. 1.0 M $HClO_4$ in AN/H_2O 40/60 (v/v). $v = 20$ mV s^{-1}.

To further support film formation FTIR and reflectance spectra covering the u.v.–vis. and near i.r. regions, before and after blocking of the electrode surface, were recorded. The FTIR spectra of pure RuO_2 and IrO_2 were recorded using the oxides pressed in a KBr matrix. In the presence of organic substrate the electrodes were submitted to 50 potential cycles and after exhaustively washing with mixed solvent, to remove any excess of organic substrate, the electrode coating was scrapped from the Ti-support and a KBr pellet was prepared with this material. Representative FTIR spectra form pure oxide coating and with the organic film are shown in Figure 9.

Pure RuO_2 shows intense peaks at 3400, 1630 and 600 cm^{-1} characteristic of –OH (oxide hydration) [30]. The FTIR spectra of blocked RuO_2 shows bands at 2900, 1600, 1500 and 1440 cm^{-1}, characteristic of C–H and C=C axial deformation in the aromatic ring, besides bands at 1245 and 1040 cm^{-1} characteristic of C–O–C axial deformation.

Reflectance electronic spectra were recorded directly from the Ti-supported coatings after the same treatment described above. Representative spectra are shown in Figure 10. The reflectance electronic spectra of clean Ti/RuO_2 coating shows a well-defined peak at 590–

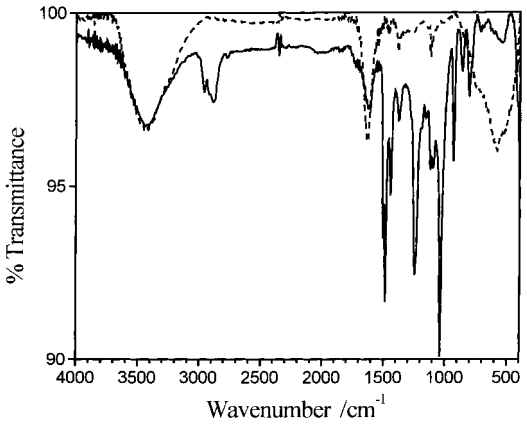

Fig. 9. FTIR spectra of RuO_2 (- - - - -) before and (——) after film formation in 36 mM ISF in 1.0 M $HClO_4$ in AN/H_2O 40/60 (v/v).

600 nm together with a shoulder centred at 430 nm. No peak is observed with pure clean Ti/IrO_2 coating. After film formation the electronic spectra shows some drastic changes. In the case of the Ti/RuO_2 electrode, depending on the region of the electrode surface sampled, intense bands (450 and 690 nm) and shoulder (640 nm) were observed. For Ti/IrO_2 electrode bands at 430 and 554 nm were observed showing that some organic material may be present on the electrode surface. We were not able to deduce the structure from these data. However the FTIR spectroscopic results clearly show that an organic substrate, similar but not identical to the original, covers the electrode surface.

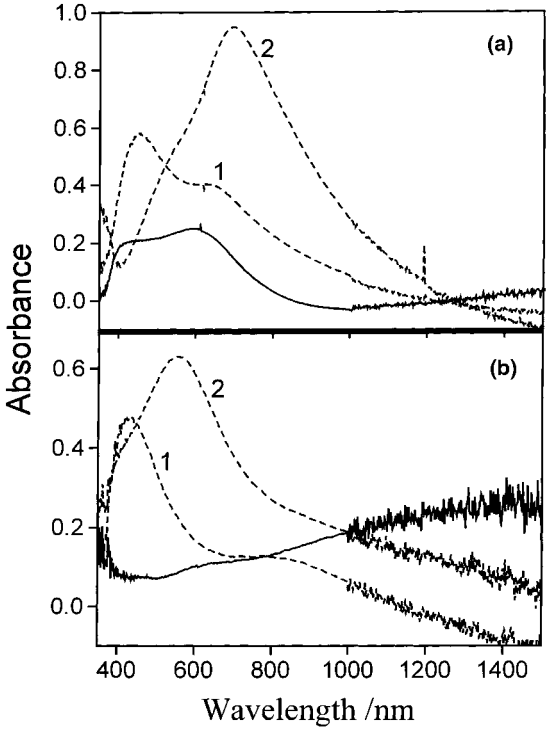

Fig. 10. Reflectance electronic spectra of: (a) Ti/RuO_2; (b) Ti/IrO_2. (——) before and (- - - - -) after film formation in 36 mM ISF in 1.0 M $HClO_4$ in AN/H_2O 40/60 (v/v). Curves 1 and 2 registered in different regions of the electrode surface.

It is well known that the ohmic resistance, R_Ω, is a parameter which mainly describes the resistance of the solution contained between the working electrode and the tip of the Luggin capillary. Therefore, if an extra resistive element is incorporated in this region (e.g., a film blocking the electrode surface) the R_Ω-value must increase. This hypothesis was checked taking impedance measurements in 1.0 M $HClO_4$ aqueous solution, from which R_Ω was determined, before and after surface blocking of the Ti/RuO_2 electrode. Before electrode blocking a 0.4 $\Omega\,cm^{-1}$ value for R_Ω was obtained which is typical for DSA® electrodes in 1.0 M $HClO_4$ and in good agreement with the results of earlier investigations [31, 32]. After electrode blocking, as described before for FTIR experiments, the impedance measurements furnished a R_Ω- value of 1.7 $\Omega\,cm^{-1}$. After elimination of the blocking film, washing the electrode abundantly with AN and holding the potential applied at 1.7 V vs NHE for a few minutes, the R_Ω returned to its original value (0.4 $\Omega\,cm^{-1}$) supporting the complete recovery of the electrode surface. These findings strongly support surface blocking is mainly caused by film formation due to dimerization/polymerization of the cation radical formed.

Depending on the structure of the organic substrate and electrolysis conditions, blocking of the electrode activity may be rather unimportant, permitting electrosynthesis to be carried out. This is the case for benzyl alcohol oxidation on Ti/RuO_2 [5] for which a 65–85% benzaldehyde yield was obtained. In the present investigation, however, with the electrolysis carried out at peak potential, electrode deactivation is so effective that the faradaic current falls to residual current values after a few minutes of electrolysis. Presently studies are under way to avoid electrode deactivation making electrosynthesis experiments possible.

4. Conclusion

The aliphatic olefins CH and IF are electrochemically inactive in the potential region preceding the OER on Ti/MO_2 and Ti/$M_{0.3}Ti_{0.7}O_2$ (M = Ru or Ir) metallic conductive oxide electrodes. In the same potential region, the aromatic olefins are oxidised in a single (SF) or two (ISF) steps showing a dependence on substrate structure. The faradaic current density suggests that the oxidation process for both substrates occurs with the same number of electrons. The catalytic species in the case of Ru-based electrodes is the ruthenate (Ru(VI)) species while for the Ir-based electrodes species with higher oxidation state than Ir(IV) may be involved. The several electrode materials tested showed a significant difference in the number of electrochemically active surface sites. Nevertheless, for the oxidation of the organic substrates investigated, a diffusion controlled process, the overall efficiency is independent from the number of electrochemical active surface site.

Partial substitution of the catalysts by TiO_2 revealed an inhibition (depressive action) of the catalytic activity of the TiO_2-stabilized electrode material. The decrease in current observed on continuous potential cycling is attributed to dimeric/polymeric film formation blocking the electrode surface. Evidence for film formation was obtained from spectroscopic data (FTIR and reflectance spectra) and from ohmic resistance values.

Acknowledgements

A.R. de Andrade and C.L.P.S. Zanta wish to acknowledge financial support received from the FAPESP foundation. J.F.C. Boodts thanks the FAPEMIG and CAPES Foundations.

References

1. S. Trasatti, 'Electrodes of Conductive Metallic Oxide', Part A and B Elsevier Scientific Publishing, Amsterdam, 1980/1981.
2. E.J.M. O'Sullivan and J.R. White, *J. Electrochem. Soc.* **136** (1989) 2576.
3. M.E.G. Lyons, C.H. Lyons, A. Michas and P.N. Bartlett, *J. Electroanal. Chem.* **351** (1993) 245.
4. K. Asokan and V. Krishnan, *Bull. Electrochem.* **4** (1988) 827.
5. S.M. Lin and T.C. Wen, *J. Appl. Electrochem.* **25** (1995) 73.
6. D.T. Shieh and B.J.Hwang, *J. Electrochem. Soc.* **142** (1995) 816.
7. C. Comninellis and A. De Battisti, *J. Chim. Phys.* **93** (1996) 673.
8. O. Simond, V. Schaller and C. Comninellis, *Electrochim. Acta* **42** (1997) 2009.
9. L.D. Burke and O.J. Murphy, *J. Electroanal. Chem.* **109** (1980) 199.
10. L.D. Burke and J.F. Healy, *J. Electroanal. Chem.* **124** (1981) 327.
11. L.D. Burke and M.Mc Carthy, *Electrochim. Acta* **29** (1984) 211.
12. R. Kotz and S. Stucki, *Electrochim. Acta* **31** (1986) 1311.
13. A.M. Couper, D. Pletcher and F.C. Walsh, *Chem. Rev.* **90** (1990) 837.
14. D. Galizzioli, F. Tantardini and S. Trasatti, *J. Appl. Electrochem.* **5** (1975) 203.
15. R. Kötz, S. Stucki and B. Carcer, *J. Appl. Electrochem.* **21** (1991) 14.
16. S. Stucki, R. Kötz, B. Carcer and W. Suter, *J. Appl. Electrochem.* **21** (1991) 99.
17. C. Comninellis and A. Nerini, *J. Appl. Electrochem.* **25** (1995) 23.
18. S. Ye and F. Beck, *Electrochim. Acta* **36** (1991) 597.
19. N.T. Farinacci, *US Pat. 2 794 813* (1957); *Chem. Abstr.* **51**, 6572 (1957); A.V. Bogastskii, A.P. Antonov, Y.V. Gavyevich, V.V. Titor and V.Y. Kalashnikov, *USSR Pat. 490 793* (1975); *Chem. Abstr.* **84**, 74254 (1976).
20. J.M. Madurro, G. Chiericato, W.F. de Giovani and J.R. Romero, *Tetrahedron Lett.* **29** (1988) 765.
21. J. Grimshaw and C. Hua, *Electrochim. Acta* **39** (1994) 497.
22. R. Garavaglia, C.M. Mari and S. Trasatti, *Surf. Technol.* **23** (1984) 41.
23. D. Galizzioli, F. Tantardini and S. Trasatti, *J. Appl. Electrochem.* **4** (1974) 57.
24. L.D. Burke and O.J. Murphy, *J. Electroanal. Chem.* **96** (1979) 19.
25. S. Ardizzone, G. Fregonara and S. Trasatti, *Electrochim. Acta* **35** (1990) 263.
26. T.C. Wen and C.C. Hu, *J. Electrochem. Soc.* **139** (1992) 2158.
27. L.A. da Silva, V.A. Alves, M.A.P. da Silva, S. Trasatti and J.F.C. Boodts, *Can. J. Chem.* **75** (1997) 1483.
28. C.P. De Pauli and S. Trasatti, *J. Electroanal. Chem.* **396** (1995) 161.
29. G.N. Martelli, R. Ornelas and G. Faita, *Electrochim. Acta* **11–12** (1994) 1551.
30. A. Bewich, C. Gutiérres and G. Larramona, *J. Electroanal. Chem.* **332** (1992) 155.
31. L.A. da Silva, V.A. Alves, M.A.P. da Silva, S. Trasatti and J.F.C. Boodts, *Electrochim. Acta* **42** (1997) 271.
32. V.A. Alves, L.A. da Silva and J.F.C. Boodts, *J. Appl. Electrochem.* **28** (1998) 899.